




# A multi-channel localized surface plasmon resonance system for absorptiometric determination of abscisic acid by using gold nanoparticles functionalized with a polyadenine-tailed aptamer

Shun Wang<sup>1,2</sup> · Hao Zhang<sup>2</sup> · Wei Li<sup>1,3</sup> · Zephania Birech<sup>4</sup> · Liuzheng Ma<sup>2</sup> · Dongxian Li<sup>2</sup> · Shixin Li<sup>2</sup> · Ling Wang<sup>2</sup> · Junjuan Shang<sup>2</sup> · Jiandong Hu<sup>2,3</sup> 

Received: 1 July 2019 / Accepted: 3 November 2019 / Published online: 5 December 2019  
© Springer-Verlag GmbH Austria, part of Springer Nature 2019

## Abstract

A multi-channel localized surface plasmon resonance system is described for absorptiometric determination of abscisic acid (ABA). The system is making use of gold nanoparticles and consists of a broadband light source, a multi-channel alignment device, and a fiber spectrometer. The method is based on the specific interaction between an ABA-binding aptamer and ABA. This induces the growth of gold nanoparticles (AuNPs) functionalized with a polyadenine-tailed aptamer that act as optical probes. Different concentrations of ABA give rise to varied morphologies of grown AuNPs. This causes a change of absorption spectra which is recorded by the system. ABA can be quantified by measurement of the peak wavelength shifts of grown AuNPs. Under optimized conditions, this method shows a linear relationship in the 1 nM to 10  $\mu$ M ABA concentration range. The detection limit is 0.51 nM. The sensitivity of the ABA assay is strongly improved compared to the method based on salt-induced AuNP aggregation. This is attributed to the use of a poly-A-tailed aptamer and the catalytic ability of AuNPs. In the actual application, the ABA concentration of ABA in fresh leaves of rice is measured with the maximum relative error of 8.03% in comparison with the ELISA method.

**Keywords** Aptamer-AuNPs probes · Catalytic growth · Alignment device · Fiber spectrometer · Plant hormone · Varied morphologies · Absorption spectra · Peak wavelength shift

## Introduction

Abscisic acid (ABA) is a plant hormone that improves a plant's tolerance to adverse environmental effects besides maintenance of bud and seed dormancy. Generally, ABA controls growth

and development of plants including seed maturation, root formation and leave size among others [1]. Therefore, detection of ABA concentration can provide information about a plant's health and its ability to cope with stress. Traditional ABA detection involves spectroscopic [2, 3], electrochemical [4, 5] and chromatographic methods such as high-performance liquid chromatography (HPLC) [6] and liquid chromatography/mass spectrometry (LC/MS) [7–9]. However, some of these methods require large-scale instruments and use of antibodies with complicated preparation procedures. For further investigation of plant hormone regulation and signal transduction, some approaches with high sensitivity and specificity for ABA detection are strongly desired.

Colorimetric and light scattering methods based on localized surface plasmon resonance (LSPR) have been often used to quantify a variety of analytes that range from small molecules and ions [10, 11], proteins [12], nucleic acids [13], food contaminants [14, 15] to diagnostic compounds [16–18]. Approaches have been used to measure the LSPR also include reflection spectroscopy and dark-field imaging

---

**Electronic supplementary material** The online version of this article (<https://doi.org/10.1007/s00604-019-4003-7>) contains supplementary material, which is available to authorized users.

---

✉ Jiandong Hu  
jiandonghu@163.com

- <sup>1</sup> College of Science, Henan Agricultural University, Zhengzhou 450002, China
- <sup>2</sup> College of Mechanical and Electrical Engineering, Henan Agricultural University, Zhengzhou 450002, China
- <sup>3</sup> State Key Laboratory of Wheat and Maize Crop Science, Zhengzhou 450002, China
- <sup>4</sup> Department of Physics, University of Nairobi, Nairobi 30197, Kenya

[19]. Among these spectral measurements, transmission spectroscopy is used in routine analysis to record the absorption spectra when the incident light interacts with the nanoparticles. In our group, we demonstrated a LSPR approach involving salt-induced aggregation of gold nanoparticles (AuNPs) for detection of ABA with the detection limit of  $\mu\text{M}$  order [20]. The method exploited aptamer as the specific recognition element and AuNPs as the probe. The spectra were acquired through a commercial UV-Vis spectrometer. For most commercial UV-Vis spectrometers, however, spectral signal acquisition needs a process of wavelength scanning, which makes the measurements time-consuming. Several optical fiber techniques have received great attentions for fast spectral signals acquisition [21–24]. The changes in absorption spectra can be monitored using an optical fiber spectrometer, which eliminates the need for scanning.

The combination of DNA and AuNPs have been widely utilized for biosensing materials and strategies [25–27]. Studies have found that the base adenine (A), thymine (T), cytosine (C) and guanine (G) of DNA have different affinity towards the surface of AuNPs, where the binding affinity of base A is higher than the others [28, 29]. Depending on the strong affinity of polyA sequence to AuNPs, the polyA-tailed aptamer conjugated to AuNPs provide a novel analytical approach. This makes the conjugation process of DNA and AuNPs convenient and effective [30, 31]. When DNA is attached on the AuNP surface, the physicochemical properties including catalytic ability of bare AuNPs are changed. The sequence-dependent affinity between DNA and AuNPs can be used to mediate the catalytic growth of AuNPs. This result in different morphologies and colour appearance, which corresponds to different absorption bands [32–36]. Aptamers are single-stranded DNA/RNA and well-known as alternatives to antibodies. They are widely used as recognition elements in biosensing analysis due to the advantages of small molecular weight, non-immunogenicity, and easy modification [37, 38].

In this work, we mainly focus on (i) constructing a multi-channel LSPR biosensing system for rapid acquisition of spectral signal; (ii) investigating different aptamer-functionalized AuNPs probe and selecting an optimized favorable AuNP probe for ABA detection with high sensitivity. It is already known that the catalytic ability of bare AuNPs are changed when their surfaces are attached with aptamers. The approach employed here for ABA detection utilizes polyA-tailed aptamer and the catalytic growth of aptamer-functionalized AuNPs. The grown AuNPs exhibited different morphologies and colour variations with different concentration of ABA. They were then characterized by the biosensing system and transmission electron microscopy (TEM). Compared with salt-induced gold nanoparticles aggregation methods and commercial instruments, this work demonstrated an improved strategy for ABA detection with high sensitivity.

## Experimental

### Materials and reagents

PolyA-tailed aptamers were synthesized by Sangon Biotechnology Co., Ltd. (Shanghai, China, [www.sangon.com](http://www.sangon.com)) (Table 1 and Table S1). 5 nm AuNPs were purchased from BBI Solutions (Cardiff, UK, [www.bbisolutions.com](http://www.bbisolutions.com)). ( $\pm$ )-Abscisic acid ( $\pm$ -ABA), Gibberellic acid ( $\text{GA}_3$ ), and 3-Indoleacetic acid (IAA) were purchased from Sigma-Aldrich Co., Ltd. (USA, [www.sigmaaldrich.com](http://www.sigmaaldrich.com)). Tetrachloroauric (III) acid tetrahydrate ( $\text{HAuCl}_4 \cdot 4\text{H}_2\text{O}$ ) and Hydroxylamine ( $\text{NH}_2\text{OH}$ ) were purchased from Sinopharm Chemical Reagent Co., Ltd. (Shanghai, China, [www.sinoreagent.com](http://www.sinoreagent.com)). Methanol, formic acid and acetic acid were purchased from Shanghai Aladdin biological technology Co. Ltd. (China, [www.aladdin-e.com](http://www.aladdin-e.com)). ABA commercial ELISA kits were purchased from Shanghai MLBIO Biotechnology Co., Ltd. (Shanghai, China, [www.mlbio.com](http://www.mlbio.com)). Fresh leaves of rice were provided by Agronomy College of Henan Agricultural University. Ultra-pure water was used throughout the experiment.

### Construction of a multi-channel biosensing system

The schematic of a multi-channel LSPR biosensing system in a transmission mode is shown in Fig. 1, which consisted of a tungsten halogen lamp (HL-200, Ocean Optics), a fiber optic variable attenuator, three multimode optical fibers, two 74-UV collimation lens, a fiber spectrometer (USB2000+, Ocean Optics), and a home-made multi-channel alignment device. From Fig. 1a, the incident light in the spectral range 360–2000 nm was emitted by the tungsten halogen lamp and then adjusted to a suitable intensity by the attenuator. Then the light was focused onto the samples inside the multi-channel device with the assistance of a 74-UV collimation lens. Thereafter, the other 74-UV collimation lens was used to collect the transmission light. Finally, the transmitted light was dispersed in the fiber spectrometer and the absorption spectra were displayed.

Figure 1b depicts the multi-channel alignment device. It includes two sliding plates that can be moved along the reciprocal vertical guided rail (in both the X and Y direction). The two sliding directions (i.e. X and Y) were achieved with the help of 12 and 8 positioning holes designed on the guided rails, respectively. This device can fully match the commercial 96-well plates. Two steel balls and mechanical springs were embedded inside the positioning holes of the both rails. When the guided rail moves forward a certain distance, a steel ball is impelled into the positioning hole by the elasticity of the spring. Upon reaching the terminal positioning hole (i.e. the guided rail),

**Table 1** Sequences of the aptamers with different polyA tail at the 5'- position

Name	Sequences (5'-3')
Apt-5'-2A	AAATGGGTTAGGTGGAGGTGGTTATTCCGGGAATTCGCCCTAAATACGAGCAAC
Apt-5'-3A	AAAATGGGTTAGGTGGAGGTGGTTATTCCGGGAATTCGCCCTAAATACGAGCAAC
Apt-5'-4A	AAAAATGGGTTAGGTGGAGGTGGTTATTCCGGGAATTCGCCCTAAATACGAGCAAC
Apt-5'-5A	AAAAAATGGGTTAGGTGGAGGTGGTTATTCCGGGAATTCGCCCTAAATACGAGCAA C

it will hit the block and is stopped. Consequently, precise positioning is realized. To investigate the effect of different positions, the following experiments were carried out. The spectra of 13.5 nm AuNPs samples were recorded at different positions of the 96-well plates and the spatial distribution of absorbance at 520 nm is shown in Fig. S1. The results demonstrated that there was good consistency among the different positions of the multi-channel system.

### Preparation of aptamer-functionalized AuNPs probes

The 5 nm AuNPs were conjugated with ABA aptamers which possesses different sequences and polyA tails. Before conjugation, the aptamers were annealed at 95 °C for 5 min and then

cooled in ice bath for another 5 min. After that, 10  $\mu\text{L}$  of 1  $\mu\text{M}$  aptamers were incubated with 3.75  $\mu\text{L}$  AuNPs (8.3 nM) at room temperature overnight. To obtain a final constant volume of 180  $\mu\text{L}$ , corresponding volumes of ultra-pure water were added.

### Catalytic growth of polyA-tailed aptamer-functionalized AuNP probe for improved ABA detection

After the functionalized-AuNPs probes were synthesized, 20  $\mu\text{L}$  of different concentrations of ABA were added. Then, 5  $\mu\text{L}$   $\text{NH}_2\text{OH}$  (400 mM) and 10  $\mu\text{L}$   $\text{HAuCl}_4$  (1.9 mM) were added to initiate the catalytic growth of AuNPs. After the AuNPs have been thoroughly mixed, incubation was performed again for another 5 min. An amount of 10  $\mu\text{L}$  chloroauric acid (1.9 mM) was repeatedly added for three times since the catalytic growth of the probe stopped at a volume of 40  $\mu\text{L}$   $\text{HAuCl}_4$  (1.9 mM), see Fig. S2. Finally, the samples were arranged to acquire the absorption spectra.

### Sample pretreatment

The pretreatment procedures of fresh leaves of rice are listed as follows. (i) 100 mg of fresh leaves were cut into a number of small pieces and kept in a 2 mL centrifuge tube. (ii) the small pieces were ground using liquid nitrogen with the help of steel balls and then it was performed with a 30 min ultrasound treatment after adding 200  $\mu\text{L}$  methanol-water-formic acid solution (15:4:1, v/v/v). (iii) the formed mixture was centrifuged for 15 min (10,000 rpm, 4 °C) and then the supernatant was kept in a 1.5 mL centrifuge tube. (iv) the residues at the bottom of centrifuge tube was extracted for twice with 100  $\mu\text{L}$  of methanol-water-formic acid (15:4:1, v/v/v) and the supernatant was also transferred to the above 1.5 mL centrifuge tube. (v) the supernatant was filtered with 0.22  $\mu\text{m}$  filter membrane. (vi) the filtrate was dried by nitrogen and then dissolved with 500  $\mu\text{L}$  methanol-water-acetic acid (90:10:0.05, v/v/v) for future analysis.

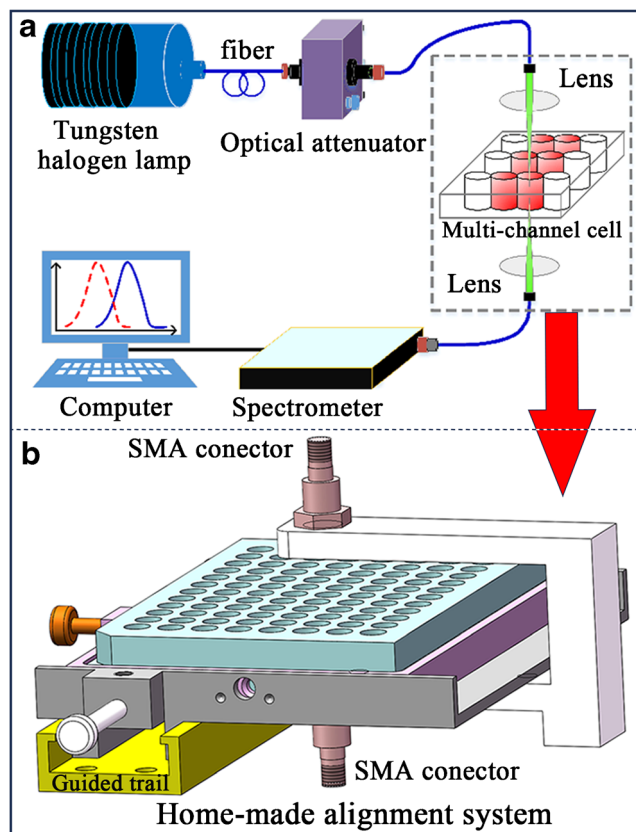


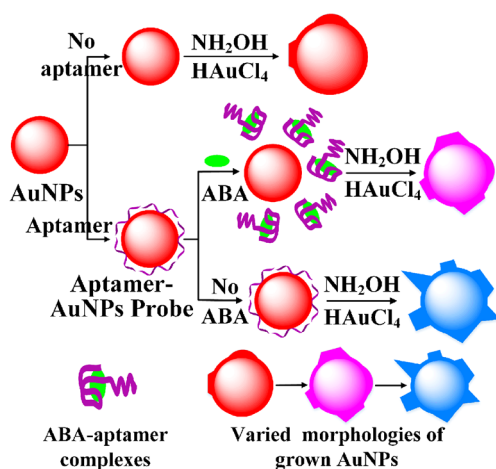
**Fig. 1** Schematic of the multi-channel LSPR biosensing system (a) and the multi-channel alignment device (b)

## Results and discussion

### Detection principle of ABA

The principle of our detection approach for ABA is shown in Scheme 1. Due to the physical adsorption [39, 40], the aptamer for ABA was attached onto the surface of AuNPs and forming an aptamer-functionalized AuNPs probes. In the presence of ABA, the aptamer conformation changed into a G-quadruplex-like structure and specifically bound with ABA. This results in desorption of aptamers onto the surface of AuNPs. The amount of aptamers attached onto the surface of AuNPs depended on ABA concentration. In fact, the higher the ABA concentration was added, the fewer amounts of aptamers were attached onto the surface of AuNPs. On the other hand, when ABA was absent, the aptamers remained attached onto the surface of AuNPs. The surfaces of non-aptamer attached AuNPs were completely exposed. The difference in surface state can, therefore, lead to the differences in physicochemical properties including catalytic ability of AuNPs.

Considering the above information,  $\text{NH}_2\text{OH}$ , a reducing agent, and  $\text{HAuCl}_4$ , a growth-promoting agent were sequentially added into the above solution. This initiated the catalytic growth reaction of AuNPs. During the growth process, the bare AuNPs grew into larger spherical particles and the colour appeared red. Similarly, the AuNPs with a low coverage of aptamers tended to grow into spheroidal particles. Interestingly, the AuNPs with a high coverage of aptamers was found to disturb the uniform growth of AuNPs. This results in more branches of grown AuNPs and a blue-coloured solution, as demonstrated by the LSPR spectra and TEM images. In brief, upon the addition of different concentration of ABA, the catalytic growth of aptamer-functionalized AuNPs probes generated morphologically varied nanostructures with different colours and LSPR spectra, thereby achieving detection of ABA.



**Scheme 1** Schematic illustration of the principle for ABA detection

To further demonstrate the possibility of the detection approach, the catalytic growth of AuNPs was implemented under different experimental conditions (see Fig. 2). As conceived, the colour of bare AuNPs after catalytic growth appeared red and the TEM image displayed a spherical morphology (see inset (I) in Fig. 2a and b). However, the colour of grown AuNPs with attached aptamer and without ABA was blue and a branched morphology was acquired (as shown in inset (II) of Fig. 2a and b). Differently, the colour of grown AuNPs with attached aptamer and ABA was purple and the TEM image showed a less branched morphology (see inset (III) in Fig. 2a and b). Accordingly, the colour and morphological changes of the grown AuNPs were characterized by the LSPR spectra, which were quickly recorded by the multi-channel LSPR system and a blue shift was observed (as shown in Fig. 2c).

### The modified aptamer-functionalized AuNPs probe

For the ABA aptamer with no polyA tail, the peak wavelength shift with respect to the blank ( $\Delta\lambda$ ) was 3.04 nm for 10 nM ABA concentration, as shown in Fig. 3a. It is well known that base A has a much higher binding affinity to AuNPs [28, 29].

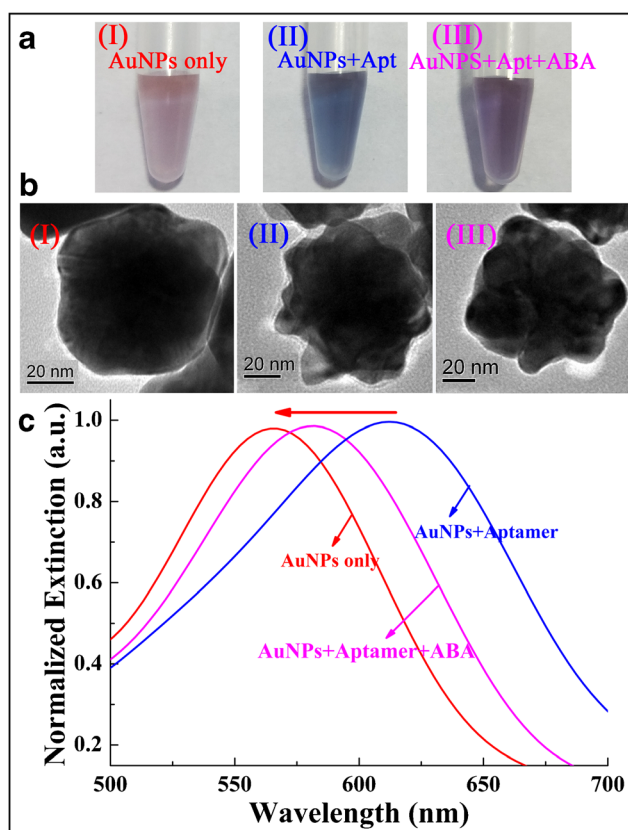


**Fig. 2** Photographs showing different colours of the grown AuNPs in the absence and presence of aptamer and ABA and aptamer only (a) and TEM images generated after the growth of 5 nm AuNPs under different conditions (b). The corresponding absorption spectra recorded by the multi-channel LSPR system (c)

We conceived that the strong interaction between polyA-tailed aptamer and AuNPs should be good for achieving a higher detection sensitivity. With the use of polyA-tailed aptamer, the acquired peak wavelength shift was 6.51 nm for the 10 nM ABA concentration (see Fig. 3b). Obviously, the use of polyA-tailed aptamer had an influence on the peak wavelength shift. In this regard, different polyA tails were added at the 5'- position and 3'- position of the aptamer sequence respectively, as listed in Table 1 and Table S1. The spectra and the peak wavelength shifts are shown in Fig. S3 and Fig. S4 for different polyA-tailed aptamers. For some aptamers with different polyA tails, the blank peak wavelength was larger than that of target. The explanation of this was that the affinity between polyA-tailed aptamer and AuNPs was higher than that of ABA and its aptamer. The results showed that the peak wavelength shift of Apt-5'-3A was largest for ABA detection among the above aptamers with different sequence, which mean that the sensitivity from Apt-5'-3A was higher. For this reason, Apt-5'-3A was selected for the subsequent studies. From the experimental results, it can be concluded that the

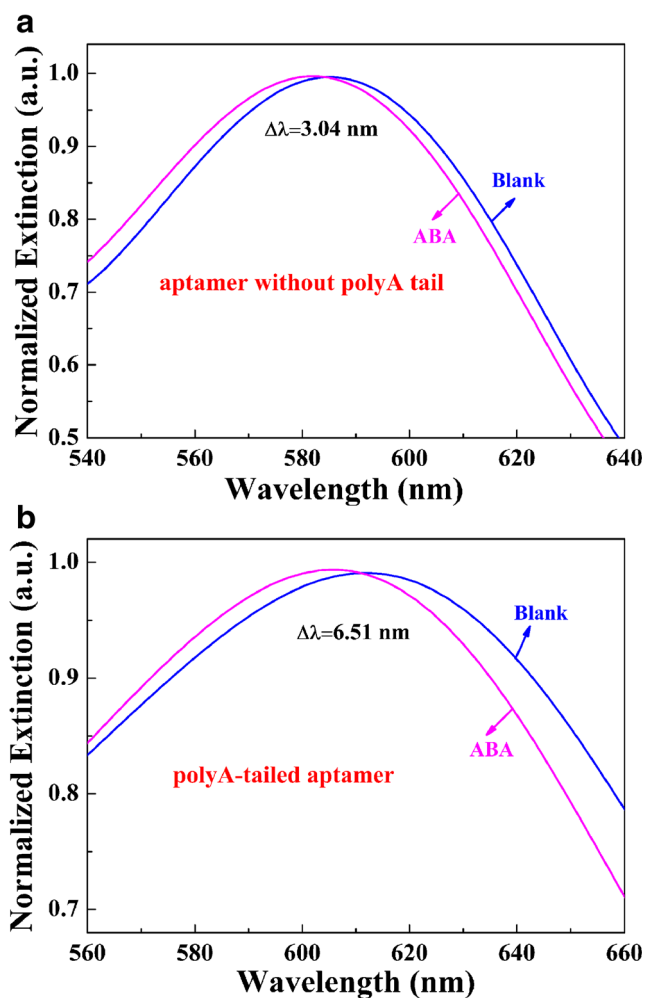


Fig. 3 Comparison for detection of ABA between the aptamer without and with polyA tail

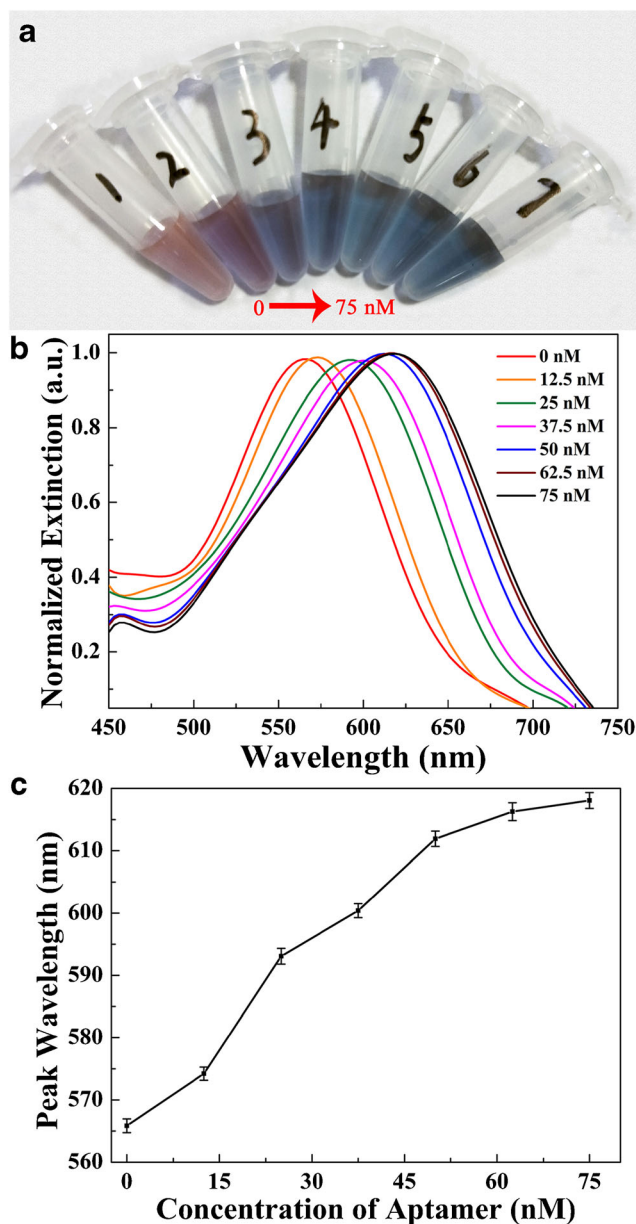
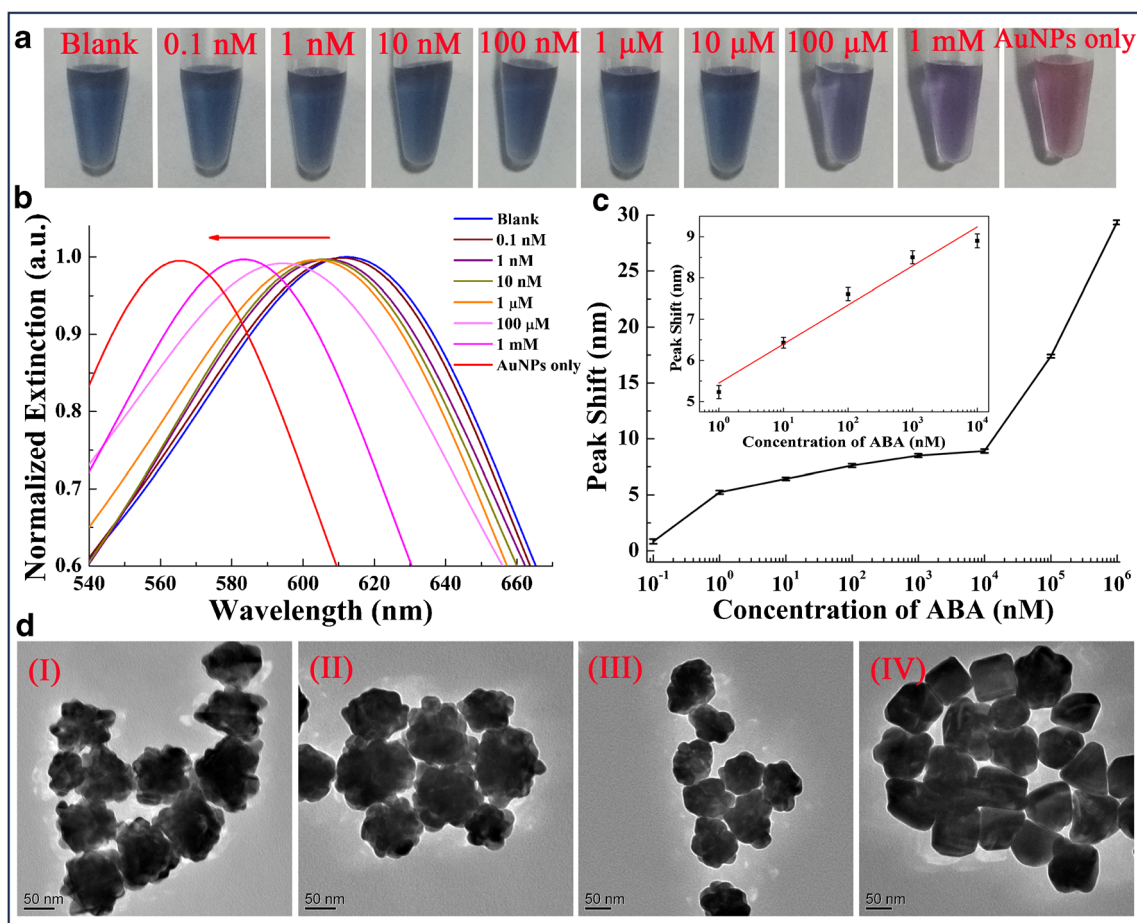


Fig. 4 a Images of different colours for grown AuNPs under different concentrations of Apt-5'-3A. b Absorption spectra, and (c) corresponding peak wavelength of grown AuNPs with an increase in the concentration of Apt-5'-3A. Error bars represent standard deviations of sample measurements ( $n = 3$ )

number of polyA tails and its position are critical for detection sensitivity.

### Optimization of polyA-tailed aptamer concentration

The influence of concentration of the selected Apt-5'-3A on AuNP growth reaction was also investigated. A series of Apt-5'-3A concentration of 0, 12.5 nM, 25 nM, 37.5 nM, 50 nM, 62.5 nM, and 75 nM were studied. As shown in Fig. 4a, different concentrations of Apt-5'-3A



**Fig. 5** **a** Photographs showing the colour of grown AuNP solution for ABA detection. **b** Absorption spectra of the grown AuNPs under different concentrations of ABA. **c** Peak shifts of various ABA concentrations with respect to the peak wavelength of blank. Inset: Calibration plot established from the peak wavelength shifts using different

concentrations of ABA samples in the range of 1 nM–10  $\mu$ M. Error bars represent standard deviations of sample measurements ( $n = 3$ ). **d** TEM images of grown AuNPs (I) Blank, (II) 10 nM ABA, (III) 1 mM ABA, and (IV) AuNPs without the attached polyA-tailed aptamer

attached on the AuNPs surface gave rise to different colours of grown AuNPs. The colour of the solutions changed from red to purple, and then to blue with increase in Apt-5'-3A concentration. When the concentration of Apt-5'-3A was beyond 50 nM, all the grown AuNPs appeared blue. Figure 4b shows the absorption spectra of the grown AuNPs using the multi-channel LSPR system. With increase of Apt-5'-3A concentration, a continuous red shift of the LSPR peak wavelength was observed (see Fig. 4b and c). Also, Fig. 4b and c shows that when the

concentration of Apt-5'-3A was greater than 50 nM, the peak wavelength increased slightly. The spectral changes were consistent with the colour changes. These results suggested that the AuNP surface was completely covered when the concentration of Apt-5'-3A reached to 50 nM. Based on these observations, the 50 nM concentration of Apt-5'-3A was selected to prepare the polyA-tailed functionalized-AuNPs probe, thereby achieving sensitive detection of ABA.

**Table 2** Analytical results of ABA in fresh leaves of rice ( $n = 3$ )

Sample	Mean value found by present method (nM)	Mean value found by ELISA method (nM)	Relative error compared with ELISA kits (%)
1	76.84 $\pm$ 1.69	71.35 $\pm$ 1.23	7.69
2	77.76 $\pm$ 2.11	71.97 $\pm$ 1.37	8.03
3	88.64 $\pm$ 1.84	82.22 $\pm$ 1.18	7.81

## Determination of ABA

Under the optimal concentration of Apt-5'-3A described above, different concentrations of ABA were detected in the range of 0.1 nM–1 mM. The Apt-5'-3A was firstly adsorbed on the surface of 5 nm AuNPs. Then the polyA-tailed aptamer-functionalized AuNP probes were incubated with different concentration of ABA. Addition of growth solution initiated the catalytic growth of AuNPs, thus obtaining grown AuNP-solutions with different colours and spectra. As shown in Fig. 5a, the colour of grown AuNPs changes from blue to purple with the increasing concentration of ABA in the range of 0.1 nM–1 mM, corresponding to blue shift of peak wavelength in LSPR spectra (see Fig. 5b and Fig. S5). Based on the spectral changes, a dose-response curve for the peak wavelength shifts ( $\Delta\lambda$ ) was drawn (Fig. 5c). As depicted in the inset of Fig. 5c, a calibration plot was established using the fitting equation  $\Delta\lambda_{\max} = 5.45085 + 0.9471 \times \log C$ . A correlation coefficient of 0.981 in the range of 1 nM–10  $\mu$ M was acquired. In the equation,  $\Delta\lambda_{\max}$  represents the peak wavelength shift with respect to the blank and  $C$  is the concentration of ABA (nM). From the calibration plot, the limit of detection (LOD) of 0.51 nM was calculated, which is determined by the formula  $3\sigma/\text{slope}$ , where  $\sigma$  is the standard deviation and slope can be acquired from the linear calibration plot. As expected, the TEM images in Fig. 5d also displayed the varied morphologies of grown AuNPs due to different concentrations of ABA. This was consistent with colour and the spectral changes. Compared with our previous study of ABA detection using salt-induced AuNPs aggregation [20], the sensitivity of this approach was improved by more than 300 times. And the LOD is much lower than some of the reported methods [2, 3, 5] (see Table S2). The results demonstrate that the absorptiometric determination approach can be used for sensitive detection of ABA without use of large-scale instruments and antibodies. This improvement can be ascribed to the use of polyA-tailed aptamer and catalytic growth of AuNPs.

In addition, to evaluate the selectivity of this method for ABA detection, the possible interference of some other plant hormones such as  $\text{GA}_3$  and IAA were also studied. As shown in Fig. S6, the peak wavelength shift is remarkable for 1 nM ABA, while smaller shifts were observed for 1  $\mu$ M  $\text{GA}_3$  and 1  $\mu$ M IAA, respectively. The results indicated that this approach satisfied specificity for the detection of ABA due to high specificity between ABA and polyA-tailed aptamer. The spectral acquisition eliminated the wavelength scanning process and can be acquired rapidly.

## ABA determination in rice leaves

To evaluate the performance of this approach in practical applications, three samples of rice leaves were chosen and the ABA

concentration was measured. In order to compare the reliability, the ABA concentration of these samples was also measured by using commercial ELISA kits. The results are summarized in Table 2. From Table 2, the maximum calculated relative error is 8.03% in comparison with the ELISA method. It can be concluded that there is good agreement existed between two methods. The results demonstrate that this absorptiometric determination approach can be used to measure ABA in real samples.

## Conclusions

A multi-channel biosensing system was constructed for absorptiometric determination of ABA. The LSPR system can rapidly acquire the spectral signals without wavelength scanning procedure. Based on the LSPR biosensing, the improved detection of ABA with high sensitivity and specificity has been achieved due to the use of polyA-tailed aptamer-functionalized AuNPs probe and catalytic growth of AuNPs. For the achievement of target detection, the design and optimization of the sequence of the used aptamer is very important. Under the optimal conditions, this approach exhibited a good linear relationship in the ABA concentration ranged from 1 nM to 10  $\mu$ M. The detection limit of 0.51 nM is lower than the salt-induced AuNPs aggregation method. As compared with the ELISA method, the ABA concentration in fresh leaves of rice has been quantified by this LSPR system with the relative errors ranged from 7.69% to 8.03%. These results demonstrate that this inexpensive and rapid multi-channel LSPR system provides great potential for biosensing applications.

**Acknowledgments** We are grateful to Professor Jihua Tang (State Key Laboratory of Wheat and Maize Crop Science) for supplying valuable information and insights into the technology of localized surface plasmon resonance. This project was financially supported by the National Natural Science Foundation of China (31671581), Natural Science Foundation of Henan Province (162300410143), the Project of the Education Department of Henan Province (16A150011, 14A210010), China Postdoctoral Science Foundation (2017 M612399), the Project of Science and Technology of Henan Province (172102310244, 182102110427, 182102110319), the Science and Technology Innovation Project of Henan Agricultural University (KJCX2016A08, KJCX2018A09), and Henan International Joint Laboratory of Laser Technology in Agriculture Sciences.

**Compliance with ethical standards** This article does not contain any studies with human participants or animals performed by any of the authors.

## References

- Gomez-Cadenas A, Vives V, Zandalinas S, Manzi M, Sanchez-Perez AM, Perez-Clemente R, Arbona V (2015) Abscisic acid: a versatile phytohormone in plant signaling and beyond. *Curr Protein Pept Sci* 16: 413–434. <https://doi.org/10.2174/1389203716666150330130102>

2. Zhou GH, Liu YZ, Luo M, Xu QF, Ji XH, He ZK (2012) Peptide-capped gold nanoparticle for colourimetric immunoassay of conjugated abscisic acid. *ACS Appl Mater Inter* 4:5010–5015. <https://doi.org/10.1021/am301380q>
3. Li YN, Wu HL, Nie JF, Li SF, Yu YJ, Zhang SR, Yu RQ (2009) Interference-free determination of abscisic acid and gibberellin in plant samples using excitation-emission matrix fluorescence based on oxidation derivatization coupled with second-order calibration methods. *Anal Methods* 1:115–122. <https://doi.org/10.1039/b9ay00048h>
4. Li YW, Xia K, Wang RZ, Jiang JH, Xiao LT (2008) An impedance immunosensor for the detection of the phytohormone abscisic acid. *Anal Bioanal Chem* 391:2869–2874. <https://doi.org/10.1007/s00216-008-2214-6>
5. Wang R, Li Y, Li Q, Shen G, Xiao L (2009) A novel amperometric immunosensor for phytohormone abscisic acid based on in situ chemical reductive growth of gold nanoparticles on glassy carbon electrode. *Anal Lett* 42:2893–2904. <https://doi.org/10.1080/00032710903201909>
6. Bosco R, Caser M, Vanara F, Scariot V (2013) Development of a rapid LC-DAD/FLD method for the simultaneous determination of auxins and abscisic acid in plant extracts. *J Agric Food Chem* 61:10940–10947. <https://doi.org/10.1021/jf4034305>
7. Izumi Y, Okazawa A, Bamba T, Kobayashi A, Fukusaki E (2009) Development of a method for comprehensive and quantitative analysis of plant hormones by highly sensitive nanoflow liquid chromatography-electrospray ionization-ion trap mass spectrometry. *Anal Chim Acta* 648:215–225. <https://doi.org/10.1016/j.aca.2009.07.001>
8. Lopez-Carbonell M, Gabasa M, Jauregui O (2009) Enhanced determination of abscisic acid (ABA) and abscisic acid glucose ester (ABA-GE) in *Cistus albidus* plants by liquid chromatography-mass spectrometry in tandem mode. *Plant Physiol Biochem* 47:256–261. <https://doi.org/10.1016/j.plaphy.2008.12.016>
9. Lu Q, Zhang W, Gao J, Lu M, Zhang L, Li J (2015) Simultaneous determination of plant hormones in peach based on dispersive liquid-liquid microextraction coupled with liquid chromatography-ion trap mass spectrometry. *J Chromatogr B* 992:8–13. <https://doi.org/10.1016/j.jchromb.2015.04.014>
10. Ma XY, Guo ZZ, Mao ZQ, Tang YG, Miao P (2018) Colourimetric theophylline aggregation assay using an RNA aptamer and non-crosslinking gold nanoparticles. *Microchim Acta* 185:33–37. <https://doi.org/10.1007/s00604-017-2606-4>
11. Prabhasha PG, Hariitha VS, Nair SS, Pilankatta R (2017) Localized surface plasmon resonance based highly sensitive room temperature pH sensor for detection and quantification of ammonia. *Sens Actuator B Chem* 240:580–585. <https://doi.org/10.1016/j.snb.2016.08.159>
12. Chang CC, Chen CP, Lee CH, Chen CH, Lin CW (2014) Colourimetric detection of human chorionic gonadotropin using catalytic gold nanoparticles and a peptide aptamer. *Chem Commun* 50:14443–14446. <https://doi.org/10.1039/C4CC06366J>
13. Kim JH, Chung BH (2011) Naked eye detection of mutagenic DNA photodimers using gold nanoparticles. *Biosens Bioelectron* 26:2805–2809. <https://doi.org/10.1016/j.bios.2010.11.019>
14. Liu BS, Huang RL, Yu YJ, Su RX, Qi W, He ZM (2018) Gold nanoparticle-aptamer-based LSPR sensing of ochratoxin A at a widened detection range by double calibration curve method. *Front Chem* 6:94. <https://doi.org/10.3389/fchem.2018.00094>
15. Manzano M, Vizzini P, Jia K, Adam PM, Ionescu RE (2016) Development of localized surface plasmon resonance biosensors for the detection of *Brettanomyces bruxellensis* in wine. *Sens Actuator B Chem* 223:295–300. <https://doi.org/10.1016/j.snb.2015.09.099>
16. Chandrawati R, Stevens MM (2014) Controlled assembly of peptide-functionalized gold nanoparticles for label-free detection of blood coagulation factor XIII activity. *Chem Commun* 50:5431–5434. <https://doi.org/10.1039/c4cc00572d>
17. Khodaveisi J, Dadfarnia S, Shabani AMH, Saberi D (2017) Colourimetric determination of nabumetone based on localized surface plasmon resonance of functionalized gold nanoparticles as a chemical sensor. *Sens Actuator B Chem* 239:1300–1306. <https://doi.org/10.1016/j.snb.2016.09.110>
18. Zhou XT, Wang LM, Shen GQ, Zhang DW, Xie JL, Mamut A, Huang WW, Zhou SS (2018) Colourimetric determination of ofloxacin using unmodified aptamers and the aggregation of gold nanoparticles. *Microchim Acta* 185:355. <https://doi.org/10.1007/s00604-018-2895-2>
19. Willets KA, Van Duyne RP (2007) Localized surface plasmon resonance spectroscopy and sensing. *Annu Rev Phys Chem* 58:267–297. <https://doi.org/10.1146/annurev.physchem.58.032806.104607>
20. Wang S, Li W, Chang KK, Liu J, Guo QQ, Sun HF, Jiang M, Zhang H, Chen J, Hu JD (2017) Localized surface plasmon resonance-based abscisic acid biosensor using aptamer functionalized gold nanoparticles. *PLoS One* 12:e0185530. <https://doi.org/10.1371/journal.pone.0185530>
21. Lee B, Park JH, Byun JY, Kim JH, Kim MG (2017) An optical fiber-based LSPR aptasensor for simple and rapid in-situ detection of ochratoxin a. *Biosens Bioelectron* 102:504–509. <https://doi.org/10.1016/j.bios.2017.11.062>
22. Wakao M, Watanabe S, Kurahashi Y, Matsuo T, Takeuchi M, Ogawa T, Suzuki K, Yumino T, Myogadani T, Saito A, Muta KI, Kimura M, Kajikawa K, Suda Y (2017) Optical fiber-type sugar chip using localized surface plasmon resonance. *Anal Chem* 89:1086–1091. <https://doi.org/10.1021/acs.analchem.6b02380>
23. Jia S, Bian C, Sun JZ, Tong JH, Xia SH (2018) A wavelength-modulated localized surface plasmon resonance (LSPR) optical fiber sensor for sensitive detection of mercury(II) ion by gold nanoparticles-DNA conjugates. *Biosens Bioelectron* 114:15–21. <https://doi.org/10.1016/j.bios.2018.05.004>
24. Liu T, Wang W, Liu F, Wang S (2018) Photochemical deposition fabricated highly sensitive localized surface plasmon resonance based optical fiber sensor. *Opt Commun* 427:301–305. <https://doi.org/10.1016/j.optcom.2018.06.075>
25. Pei H, Li F, Wan Y, Wei M, Liu H, Su Y, Chen N, Huang Q, Fan C (2012) Designed diblock oligonucleotide for the synthesis of spatially isolated and highly hybridizable functionalization of DNA-gold nanoparticle nanoconjugates. *J Am Chem Soc* 134:11876–11879. <https://doi.org/10.1021/ja304118z>
26. Soh JH, Lin Y, Rana S, Ying JY, Stevens MM (2015) Colourimetric detection of small molecules in complex matrixes via target-mediated growth of aptamer-functionalized gold nanoparticles. *Anal Chem* 87:7644–7652. <https://doi.org/10.1021/acs.analchem.5b00875>
27. Wei X, Wang Y, Zhao Y, Chen Z (2017) Colourimetric sensor array for protein discrimination based on different DNA chain length-dependent gold nanoparticles aggregation. *Biosens Bioelectron* 97:332–337. <https://doi.org/10.1016/j.bios.2017.06.020>
28. Kimura-Suda H, Petrovykh DY, Tarlov MJ, Whitman LJ (2003) Base-dependent competitive adsorption of single-stranded DNA on gold. *J Am Chem Soc* 125:9014–9015. <https://doi.org/10.1021/ja035756n>
29. Zhang X, Liu B, Servos MR, Liu J (2013) Polarity control for nonthiolated DNA adsorption onto gold nanoparticles. *Langmuir* 29:6091–6098. <https://doi.org/10.1021/la400617u>
30. Pei H, Zuo X, Zhu D, Huang Q, Fan C (2014) Functional DNA nanostructures for theranostic applications. *Acc Chem Res* 47:550–559. <https://doi.org/10.1021/ar400195t>
31. Li W, Dong Y, Wang X, Li H, Xu D (2015) PolyA-tailed and fluorophore-labeled aptamer-gold nanoparticle conjugate for fluorescence turn-on bioassay using iodide-induced ligand displacement. *Biosens Bioelectron* 66:43–49. <https://doi.org/10.1016/j.bios.2014.10.047>
32. Wang Z, Zhang J, Ekman JM, Kenis PJA, Lu Y (2010) DNA-mediated control of metal nanoparticle shape: one-pot synthesis and cellular



- uptake of highly stable and functional gold nanoflowers. *Nano Lett* 10: 1886–1891. <https://doi.org/10.1021/nl100675p>
33. Zheng X, Liu Q, Jing C, Li Y, Li D, Luo W, Wen Y, He Y, Huang Q, Long YT, Fan C (2011) Catalytic gold nanoparticles for nanoplasmonic detection of DNA hybridization. *Angew Chem Int Ed* 50:11994–11998. <https://doi.org/10.1002/anie.201105121>
  34. Liu Q, Jing C, Zheng X, Gu Z, Li D, Li DW, Huang Q, Long YT, Fan C (2012) Nanoplasmonic detection of adenosine triphosphate by aptamer regulated self-catalytic growth of single gold nanoparticles. *Chem Commun* 48:9574–9576. <https://doi.org/10.1039/C2CC34632J>
  35. Wang Z, Tang L, Tan L, Li J, Lu Y (2012) Discovery of the DNA “genetic code” for abiological gold nanoparticle morphologies. *Angew Chem* 51(36):9078–9082. <https://doi.org/10.1002/ange.201203716>
  36. Khoubnasabjafari M, Samadi A, Jouyban A (2019) In-situ micro-scale spectrophotometric determination of phenytoin by using branched gold nanoparticles. *Microchim Acta* 186:422. <https://doi.org/10.1007/s00604-019-3546-y>
  37. Jayasena SD (1999) Aptamers: an emerging class of molecules that rival antibodies in diagnostics. *Clin Chem* 45:1628–1650. [https://doi.org/10.1016/S0009-8981\(99\)00154-0](https://doi.org/10.1016/S0009-8981(99)00154-0)
  38. Wang T, Chen C, Larcher LM, Barrero RA, Veedu RN (2019) Three decades of nucleic acid aptamer technologies: lessons learned, progress and opportunities on aptamer development. *Biotechnol Adv* 37:28–50. <https://doi.org/10.1016/j.biotechadv.2018.11.001>
  39. Kimura-Suda H, Petrovykh DY, Tarlov MJ, Whitman LJ (2003) Base-dependent competitive adsorption of single-stranded DNA on gold. *J Am Chem Soc* 125:9014–9015. <https://doi.org/10.1021/ja035756n>
  40. Warner MG, Hutchison JE (2003) Linear assemblies of nanoparticles electrostatically organized on DNA scaffolds. *Nat Mater* 2: 272–277. <https://doi.org/10.1038/nmat853>

**Publisher's note** Springer Nature remains neutral with regard to jurisdictional claims in published maps and institutional affiliations.